Redox Biology 24 (2019) 101186

Contents lists available at ScienceDirect

Redox Biology

journal homepage: www.elsevier.com/locate/redox

Research Paper

TLR4 participates in sympathetic hyperactivity Post-MI in the PVN by regulating NF-κB pathway and ROS production

Yu Wang[a], Hesheng Hu[b], Jie Yin[b], Yugen Shi[a], Jiayu Tan[a], Lu Zheng[a], Cailing Wang[c], Xiaolu Li[b], Mei Xue[b], Ju Liu[d], Ye Wang[b], Yan Li[d], Xinran Li[b], Fuhong Liu[d], Qiang Liu[d], Suhua Yan[a,b,*]

[a] School of Medicine, Shandong University, Jinan, China
[b] Department of Cardiology, Qianfoshan Hospital of Shandong Province, Jinan, China
[c] Department of Endocrinology, Qianfoshan Hospital of Shandong Province, Jinan, China
[d] Medical Research Center, Qianfoshan Hospital of Shandong Province, Jinan, China

ARTICLE INFO

Keywords:
Myocardial infarction
Sympathetic hyperactivity
PVN
TLR4
NF-κB
ROS

ABSTRACT

Sympathetic nerve hyperactivity is a primary reason for fatal ventricular arrhythmias (VAs) following myocardial infarction (MI). Pro-inflammatory cytokines produced in the paraventricular nucleus (PVN) post-MI are associated with sympathetic overexcitation; however, the precise mechanism needs further investigation. Our aim was to explore the mechanism of toll-like receptor 4 (TLR4) and its downstream molecular pathway in mediating sympathetic activity post-MI within the PVN. A rat MI model was developed via left anterior descending coronary artery ligation. TLR4 was primarily localized in microglia and increased markedly within the PVN at 3 days in MI rats. Sympathoexcitation also increased, as indicated by high levels of renal sympathetic nerve activity (RSNA) and norepinephrine (NE) concentration. TLR4 knockdown via shRNA microinjection to the PVN resulted in decreased activation of Fos protein (+) neurons in the PVN and peripheral sympathetic nerve activity. TLR4 knockdown also exhibited a lower arrhythmia score following programmed electrical stimulation than those treated with MI surgery only, indicating that the knockdown of TLR4 decreased the incidence of malignant ventricular arrhythmias following MI. LPS-induced inflammatory response was analyzed to explore the underlying mechanism of TLR4 in sympathetic hyperactivity. High levels of NF-κB protein, the pro-inflammatory cytokines IL-1β and TNF-α, and ROS production were observed in the LPS group. PVN-targeted injection of the NF-κB inhibitor PDTC attenuated NF-κB expression and sympathetic activity. Taken together, the results suggested that knockdown of microglial TLR4 within the PVN decreased sympathetic hyperactivity and subsequent VAs post-MI. The downstream NF-κB pathway and ROS production participated in the process. Interventions targeting TLR4 signaling in the PVN may be a novel approach to ameliorate the incidence of VAs post-MI.

1. Introduction

Fatal ventricular arrhythmias (VAs), including tachycardia (VT) and ventricular fibrillation (VF), are major causes of death in patients suffering from acute myocardial infarction (AMI). Previous studies have shown that sympathetic hyperactivity is one of the primary elements resulting in ventricular arrhythmogenesis and sudden cardiac death (SCD) in both patients and animal models of myocardial infarction [1–3]. Therefore, sympathetic nerve overexcitation induced by MI has received increasing attention.

The paraventricular nucleus (PVN) of the hypothalamus is an important contributor to sympathoexcitation in cardiovascular diseases, including MI [4,5]. The PVN can receive and integrate cardiac sympathetic activity and then reflect integrated information through relevant neural signaling pathways [6]. A large body of evidence suggests that MI-induced inflammation within the PVN contributes to sympathetic hyperactivity [7,8]. To date, however, the precise mechanism has not been explored.

Activation of innate immunity is the first line of the inflammatory response, and initiated by identification of pathogen recognition receptors (PRRs), specifically the toll-like receptors (TLRs). TLRs have 13 isoforms, and more than 30 ligands have been identified in mammalian cells, including leukocytes, cardiomyocytes, and endothelial cells [9]. Toll-like receptor 4 (TLR4) is predominately expressed in microglia in

* Corresponding author. Department of Cardiology, Qianfoshan Hospital of Shandong Province, 250014, Jinan, China.
E-mail address: yansuhua296@163.com (S. Yan).

https://doi.org/10.1016/j.redox.2019.101186
Received 5 January 2019; Received in revised form 14 March 2019; Accepted 28 March 2019
Available online 02 April 2019

the brain [10] and stimulated by appropriate ligands including microbial products or endogenous signals of tissue injury, such as debris from apoptotic and necrotic cells, heat shock proteins, and nucleic acid fragments [11,12]. Following stimulation, microglia are activated and induce a local inflammatory response [10], consequently triggering the downstream stimulation of the ubiquitous transcription factor, nuclear factor-κB (NF-κB), which initiates the transcription of pro-inflammatory mediators including tumor necrosis factor-α (TNF-α), interleukin-1β (IL-1β), and interleukin-6 (IL-6) [13]. Some investigators have demonstrated the role of TLR4 in the stroke-induced brain damage, and neurodegenerative diseases [14–16]. However, the effect of TLR4 in the regulation of sympathetic nerve activity has not been determined.

Zimmerman et al. [17] hypothesized that central neural reactive oxygen species (ROS) play an important role in the cardiovascular function and regulate central redox mechanisms, which may be involved in heart failure and hypertension. Recent studies have shown that ROS are increased in the rats' hypothalamus with hypertension, and ROS blockade reduced sympathetic activity [18–20]. One previous study demonstrated that intracerebroventricular (ICV) administration with the ROS scavenger tempol influenced central sympathetic neural circuits in a dose-dependent manner [21]. However, little is known concerning the effect of central ROS on sympathetic activity regulation post-MI.

Considerable evidence indicates that TLR4 activation can result in ROS secretion in neutrophils [22]. Furthermore, one previous study has shown that activated NF-κB in the PVN led to oxidative stress and sympathetic hyperactivity in rats with heart failure (HF) [23]. Given this background, we hypothesize that TLR4 expressed in microglia within the PVN was activated and participated in sympathetic hyperactivity post-MI via the NF-κB pathway and ROS production. In the present study, adeno-associated virus (AAV)-mediated short hairpin RNA (shRNA) was applied to silence the TLR4 gene in microglia of the PVN, to establish whether sympathoexcitation is mediated by TLR4 signaling. The outcomes of this study will contribute to a better understanding of the pathological process and help in designing new strategies to decrease the risk of VAs following MI.

2. Materials and methods

2.1. Animals

Male Sprague-Dawley rats (50–60 days postnatal, approximately 260 g; Vital river Company; Beijing, China) were housed at a room temperature of 22 °C with a 12 h-12 h light-dark cycle (light from 6:00 to 18:00) and received humane care. All the experimental protocols and procedures used in this study were performed in accordance with the Animal Care Committee of Shandong University Affiliated with Qianfoshan Hospital (Protocol number: S 030), which was in accordance with the Guidelines for the Care and Use of Laboratory Animals from the National Institutes of Health (1996, No. 85-23). The experiments were conducted after a 7-day acclimatization period.

2.2. Experimental design

Three separate experiments were conducted.

Protocol 1

Forty-three rats were divided into five groups (control, MI after 1, 3, 5, and 7 days, n = 8 in each group). The temporal expression of TLR4, NF-κB, NF-κB inhibitor-α (IkB-α), and NADPH oxidase 2 (NOX2) was detected by Western blotting. The specific methods for the MI model were established as previously described [27]. In brief, rats were anesthetized by 2% phenobarbital sodium (40 mg/kg), left thoracotomy and pericardiotomy were performed to expose the heart, and the left anterior descending coronary artery was ligated. The chest was incised, but the artery was not ligated in sham animals. A heating pad set to 37 °C was prepared for post-surgery rats to maintain body temperature.

Protocol 2

A total of 181 rats were randomly placed into four groups: (1) sham + AAV2 with a green fluorescent protein (GFP) reporter and scrambled RNA, which is a control for the shRNA virus (shCtrl), n = 36; (2) sham + AAV2 with shRNA for TLR4 (shTLR4), n = 40; (3) MI + shCtrl, n = 52; and (4) MI + shTLR4, n = 53. The rats were mounted on a stereotaxic apparatus (RWD Life Science, San Diego, CA, USA) following anaesthetization with 2% phenobarbital sodium (40 mg/kg). According to the Paxinos and Watson rat atlas (1.8 mm posterior, 0.4 mm lateral, and 7.9 mm deep to the bregma), we drilled two small holes through the top of the skull, and a pair of cannulas was inserted through the holes bilaterally into the PVN. Following 7 days of recovery, 50 nl of either shRNA control or shRNA TLR4 was injected into each PVN via a 0.5 μl microinjector connected to the cannula with a PE-10 tube. The reagents were injected at a rate of 0.1 μl/min using an infusion pump (RWD Life Science). Then, the microinjector was removed slowly after 15 min of intermittence. To ensure gene silencing efficiency, three different sequences targeting TLR4 were selected: GCATAGAGGTACTTCCTAATATTCAAGAGATATTAGGAAGTACCTCTATGCTTTTTT; GAATGCCAGGATGATGCCTCTTCAAGAGAGAGGCATCATCCTGGCATTTTTTT; GCGAGCTGGTAAAGAATTTATTCAAGAGATAAATTCTTTACCAGCTCGTTTTTT. The viral constructs were obtained from the GenePharma company (Shanghai, China), and synthesized at a titer of 1.0×10^{13} genomic particles/ml. Then, the rats received MI surgery four weeks after microinjection.

Protocol 3

Sixty-two rats were randomly divided into four groups: (1) naïve, n = 11; (2) sterile saline, n = 12; (3) lipopolysaccharide (LPS, Sigma-Aldrich, St. Louis, MO, USA, 0.5 μg/50 nl), n = 17; and (4) LPS + pyrrolidine dithiocarbamate (PDTC, Sigma-Aldrich, 5 μg/h), n = 22. The doses of reagents were applied as previously described [24,25]. Bilateral PVN cannulas were placed, and the osmotic minipumps connecting to the PVN cannulas were implanted subcutaneously for microinjection of PDTC or vehicle (artificial cerebrospinal fluid, aCSF) for 12 h directly into the bilateral PVN. Then, 50 nl of either saline or LPS was subsequently injected into each PVN. Microinjection was not conducted in the naïve group after anesthesia. Animals in the naïve, saline, and LPS groups received microinjection with the same dosage of aCSF as PDTC in the PDTC group to ensure that each rat was injected with the same dosage of reagents. The renal sympathetic nerve activity (RSNA) was recorded, and samples were collected for further analysis 12 h after LPS administration.

2.3. HRV measurements

Telemetry was performed in the rats of Protocol 2 following MI model establishment. Skin and subcutaneous tissue were separated, one electrode of the radiotelemetric transmitter (TR50B, AD Instrument, Australia) was placed to the xyphoid process on the chest, and the other electrode was fixed between the sternocleidomastoid muscles. The frequency domains were very-low-frequency (VLF; 0.05 Hz), low-frequency (LF; 0.05–0.75 Hz), and high-frequency (HF; 0.75–2.5 Hz) bands. The transmitter body was placed in the abdominal cavity. Dynamic electrocardiography (ECG) data were recorded every day for 24 h in via LabChart Pro software (AD Instruments). A minimum of 15-min ECG recording was selected from each instance to analyze the heart rate variability (HRV), and the ratio of LF to HF was calculated. Telemetry was conducted for three days and was not removed until RSNA recording.

2.4. RSNA recording

Three days after MI surgery, the rats were anesthetized and placed in the left lateral position. The renal nerve was dissected via a left flank incision free from the surrounding tissue under an anatomical microscope and hooked using a pair of bipolar silver wire recording

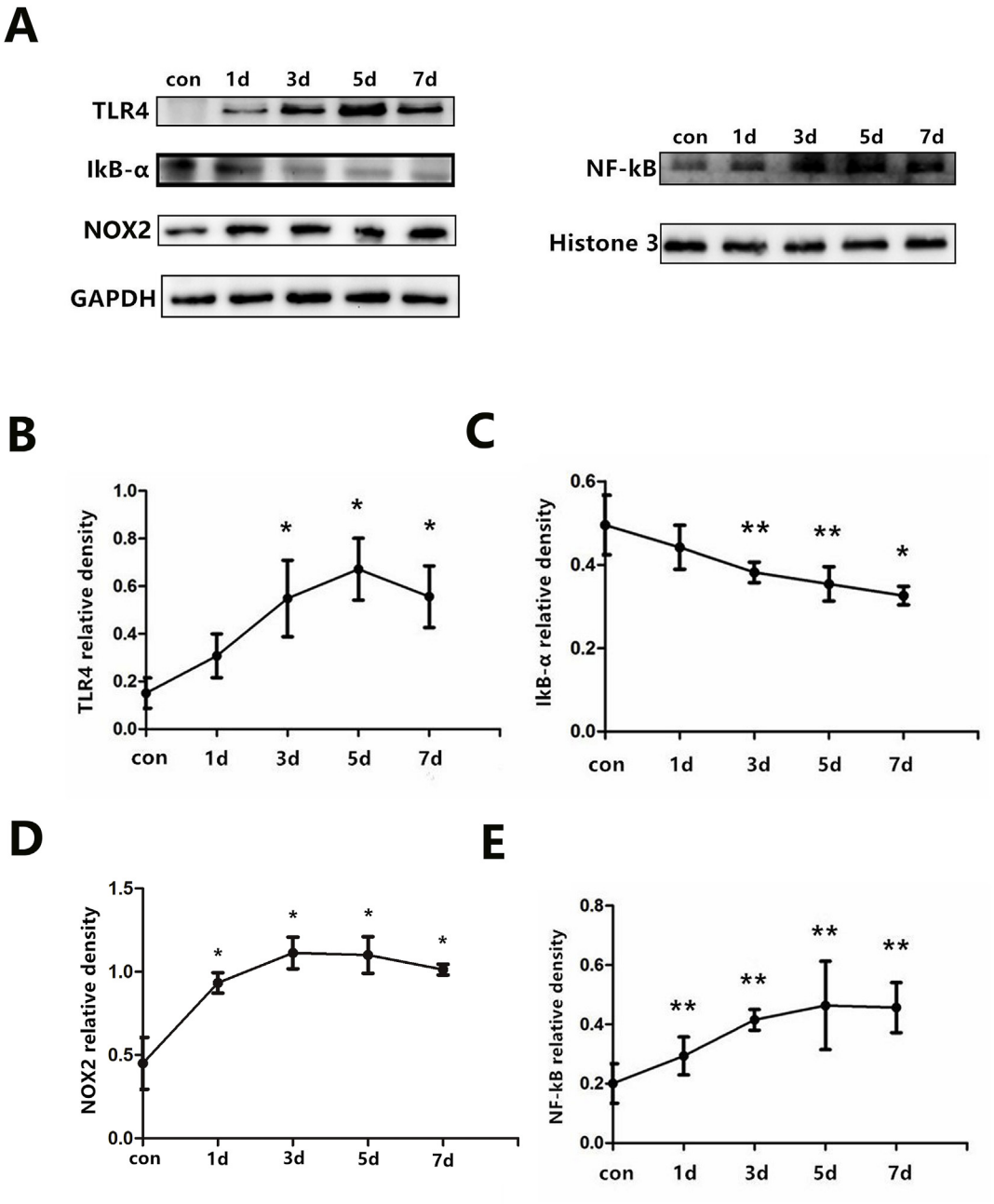

Fig. 1. (A) Protein expression profiles of TLR4 (96 kD), NF-κB (65 kD), IκB-α (36 kD), NOX2 (60 kD) within the PVN by western blot. TLR4, IκB-α, NOX2 were quantified relative to the GAPDH (37 kD) levels (B to D), and NF-κB was quantified relative to the Histone 3 (15 kD) level (E). n = 8–9 per time-point. *P < 0.01 and **P < 0.05 versus control group.

electrodes. Liquid paraffin was used to separate the electrodes and the nerve from the surrounding tissue and prevent desiccation. RSNA electrical changes were amplified, filtered, and monitored on an oscilloscope (AD Instruments, Sydney, Australia) with a frequency cutoff from 100 Hz to 3000 Hz. Data were integrated at a time constant of 10 ms with a sampling frequency at 10 kHz. Integrated RSNA was recorded simultaneously. The postmortem background data were determined and corrected for this value. Changes in RSNA were calculated as a percentage change from the baseline activity. In the representative tracings, both integrated and raw RSNA are shown, but only the integrated activity was used in the analysis [28].

2.5. In vivo electrophysiological experiments

Programmed electrical stimulation was applied according to our previous studies [29]. The rats were anesthetized, received thoracotomy, and an electric bloom stimulator (Chengdu Electronic Machine Company, Chengdu, Sichuan Province, China) was implanted to induce ventricular arrhythmias. Ventricular stimulation was performed at a basic cycle length of 150 ms (S0) followed with single (S1), double (S2), and triple (S3) additional stimuli at shorter coupling intervals. The stimulation protocols were finished within 10 min, and the arrhythmia scoring system was applied to analyze the degree of the induced VAs.

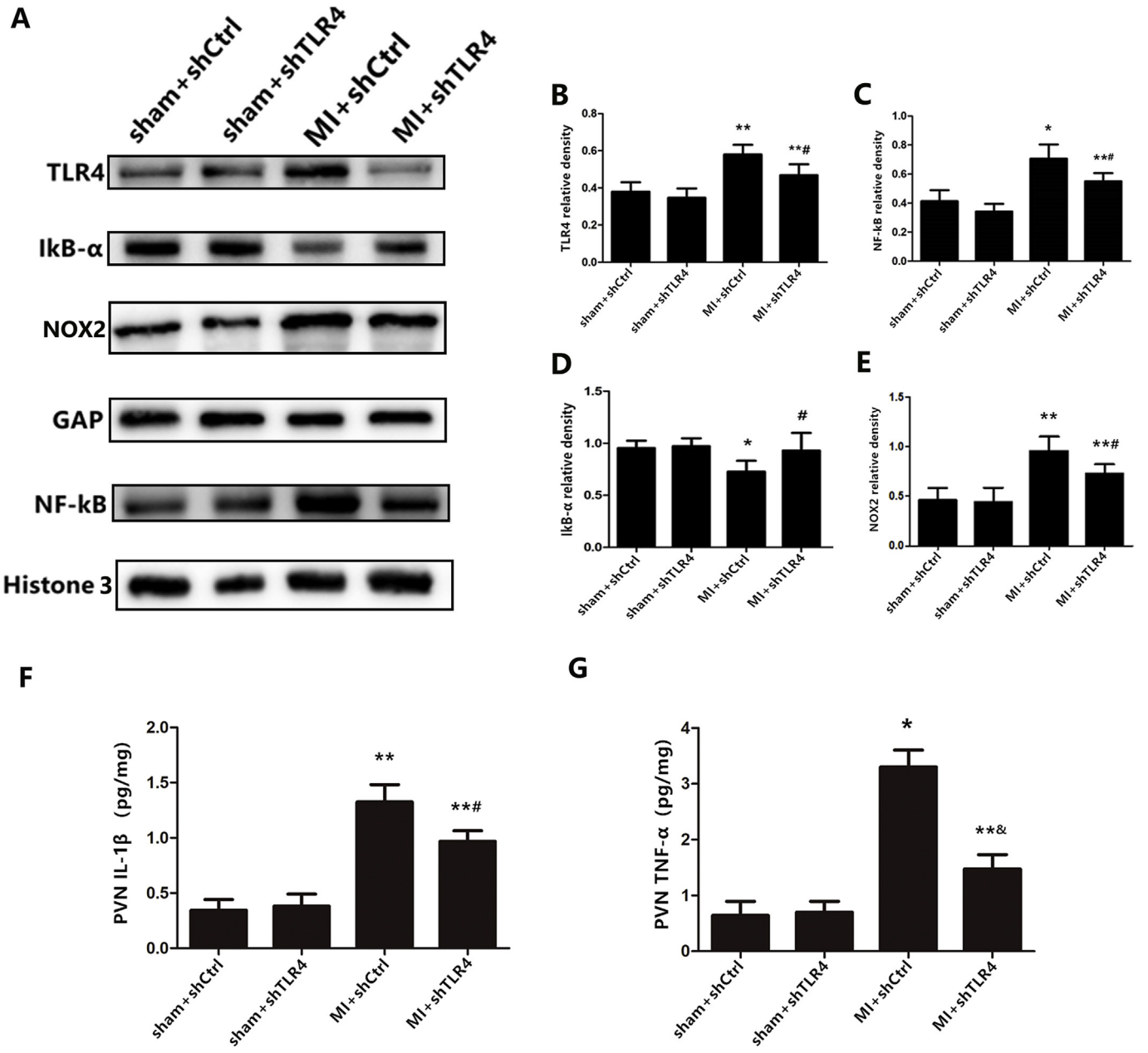

Fig. 2. (A) Representative protein expression levels of TLR4 (96 kD), NF-κB (65 kD), IκB-α (36 kD), and NOX2 (60 kD) as determined by western blot. The cytokine levels of IL-1β(F) and TNF-α(G) from the PVN tissue as measured by ELISA. n = 10–11 for each group. *P < 0.01 and **P < 0.05 versus sham groups; &P < 0.01 and #P < 0.05 versus MI + shCtrl group.

2.6. Tissue collection

The animals were sacrificed after electrophysiological study via KCl injection to the caudal veins, and then they were decapitated, and the whole brain was removed. Brain tissue was prepared using three different methods before further analysis. (1) Microinjection of methylene blue and the Paxinos and Watson rat atlas were used to determine the location of the PVN [26] (see supplemental figures). The PVN was separated from whole brain tissue and immediately stored at −80 °C for biochemical analysis. (2) The brain tissue was fixed in freshly prepared 4% paraformaldehyde for 12 h in 4 °C and then transferred to 10% neutral buffered formalin (NBF) until sectioning. (3) Whole brain tissue was embedded in Tissue-Tek® OCT compound (Sakura Finetek, Tokyo, Japan) and frozen in an isopentane liquid bath on dry ice for 10 min and then stored at −80 °C. The hearts and peripheral blood were also harvested. A mottled and pale appearance was identified as the infarcted region [27]. The myocardium extending 0.5–1.0 mm from the infarct scar was considered to represent the infarcted myocardium. Only hearts with large infarctions (> 30%) were analyzed according to clinical relevance. The middle portion of hearts stored in NBF (1.03 ± 0.21 cm thick), including the whole infarcted myocardium, was embedded in paraffin, cut into 5 μm sections, and then stained with Masson's trichrome (Jiancheng, Nanjing, China) according to standard protocols to confirm MI model establishment [31].

2.7. Immunohistochemistry

For immunohistochemical studies, brain tissue was cut into 4-μm-thick sections to measure sympathetic nerve activity via Fos family detection post-MI in the PVN. Fos family was measured using a rabbit polyclonal antibody c-fos K-25, which recognizes Fos, Fos-B, Fra-1, and Fra-2 proteins. The sections were incubated with the primary antibody:

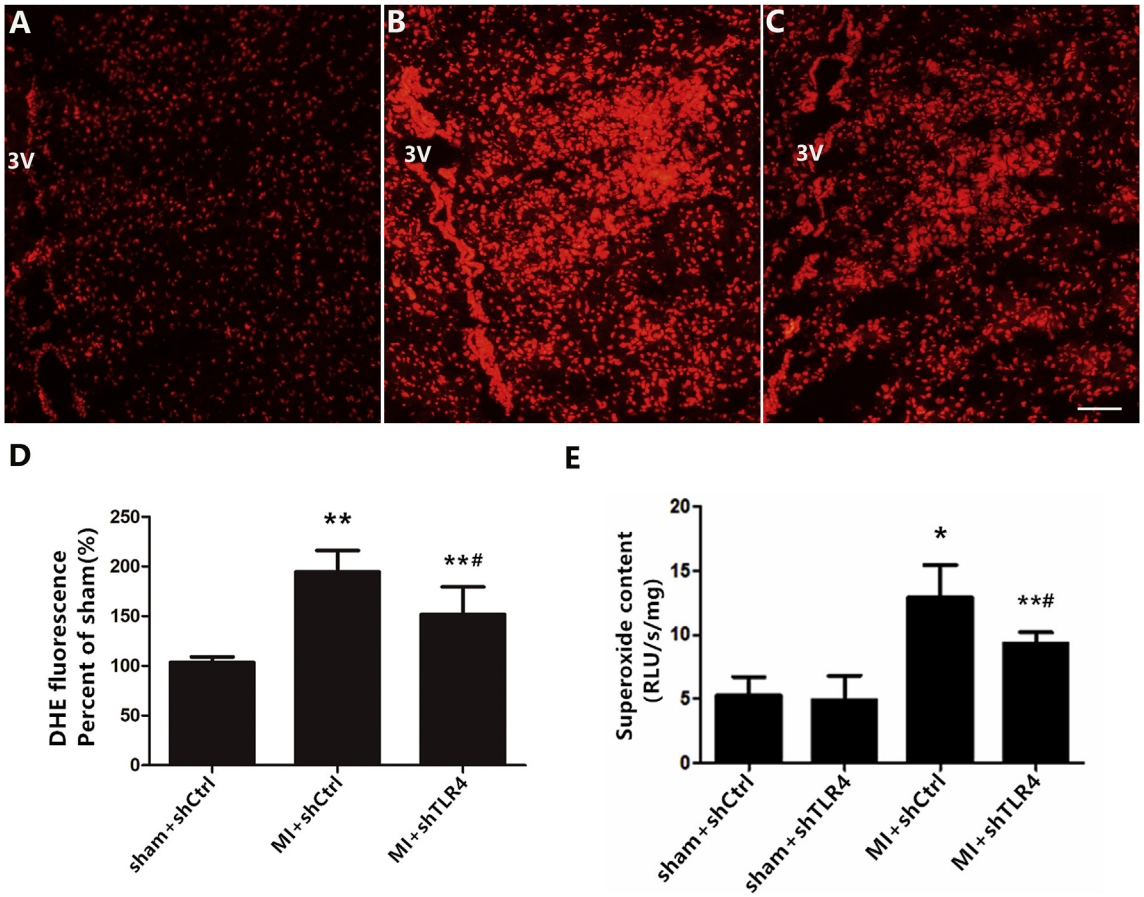

Fig. 3. Representative immunofluorescent images in rats with sham + shCtrl (A), MI + shCtrl (B) and MI + shTLR4 (C) showing DHE fluorescence in the PVN. Bar = 50 μm. D: summary of DHE fluorescence intensity in the PVN. E: Levels of superoxide content was measured via lucigenin chemiluminescence. Data are mean ± S.D as percent of the sham group. n = 10–11 in each group. *P < 0.01 and **P < 0.05 versus sham groups; #P < 0.05 versus MI + shCtrl group.

anti-*c*-fos K-25 rabbit polyclonal antibody (1:1000, Santa Cruz Biotechnology, San Francisco, CA, USA) overnight at 4 °C, and then HRP conjugated secondary antibodies: goat anti-rabbit IgG for 1 h at room temperature. The slices were incubated with DAB substrate (Solarbio Science & Technology Co., Ltd. Beijing, China) and then counterstained with hematoxylin. The digitized pictures were obtained using an Olympus LCX100 Imaging System. The number of Fos-positive cells was measured.

2.8. Immunofluorescence

Coronal sections of brain tissue (8-μm-thick) were cut using a freezing microtome (CM3050; Leica, Wetzlar, Germany). The slices were fixed with 4 °C pre-cooling acetone for 10 min, then anti-Iba-1 (1:150, Abcam, Cambridge, UK) and TLR4 (1:200, Cell Signaling Technology, Danvers, MA, USA) were used as primary antibodies overnight at 4 °C, followed by a 2 h incubation with secondary antibodies: Alexa 488-conjugated donkey anti-rabbit (1:200, Thermo Fisher, Waltham, MA, USA) and Alexa 594-conjugated donkey anti-goat (1:150, Thermo Fisher). Cell nuclei were stained with DAPI (Life Technologies, Billerica, MA, USA). The number of TLR4 or Iba-1 positive cells was calculated.

2.9. Detection of brain superoxide

Dihydroethidium (DHE) staining was used for superoxide detection. The whole brains were removed and immediately embedded in Tissue-Tek® OCT compound, after which they were frozen in an isopentane liquid bath on dry ice for 10 min. The samples were cut into 10-μm-thick sections, placed on glass slides, and incubated in 1 M DHE (Thermo Fisher, dissolved in PBS) for 30 min in a light-protected humidified chamber at room temperature. Slices were imaged using an Olympus LCX100 Imaging System and analyzed with Image J software.

In addition, lucigenin chemiluminescence was applied as an indicator of brain superoxide production. PVN samples were isolated from the brains and homogenized in PBS. Then, specimens were transferred into a polypropylene tube containing PBS-HEPES buffer and lucigenin (Sigma Aldrich, at a final concentration of 0.2 mM). Measurements were performed with an FB12-Berthold luminometer (Berthold Technologies, Bad Wildbad, Germany) at room temperature. The RLU emitted was recorded and integrated over 30-s intervals for 5 min. Activity was normalized to tissue weights.

2.10. Western blotting

The Nuclear and Cytoplasmic Protein Extraction Kit (Beyotime Institute of Biotechnology, Jiangsu, China) was used to separate nuclear and cytoplasmic proteins of PVN tissues. Nuclear protein was used for NF-κB p65 expression analysis, and cytoplasmic protein was used for TLR4, IκB-α, IL-1β, and TNF-α analysis. Protein concentrations were determined using a BCA assay kit (Pierce Protein Biology St. Louis, MO, USA). Approximately 70 μg of total protein of each sample was resolved on 6–15% polyacrylamide gels and electroblotted onto polyvinylidene difluoride membranes (PVDF membranes, Bio-Rad, Richmond, VA, USA). The membranes were incubated with different primary antibodies: anti-TLR4 rabbit polyclonal (Cell Signaling Technology, 1:1000), anti-NF-κB p65 rabbit polyclonal (Abcam, 1:1000), anti-IκB-α rabbit polyclonal (Abcam, 1:1000), anti-NOX2 rabbit monoclonal

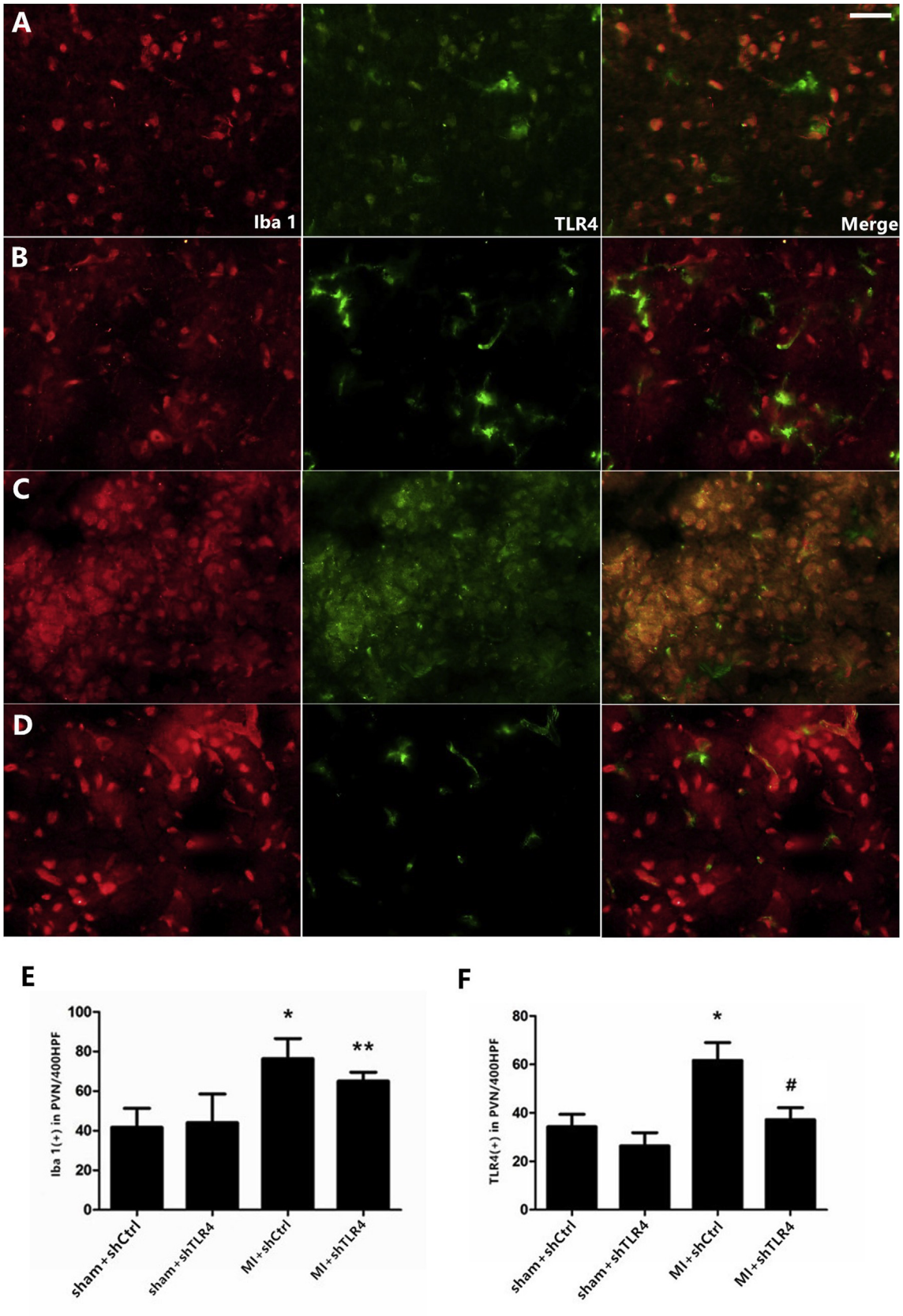

Fig. 4. Representative double-immunostaining for TLR4 (green) and Iba-1 (red) showed a limited distribution of TLR4 on microglia in the sham + shCtrl (A), sham + shTLR4 (B), MI + shCtrl (C), MI + shTLR4 (D) groups (magnification × 400). Bar = 30 μm. Quantity of TLR4-positive (E) and Iba-1-positive (F) microglia were calculated. n = 10–11 in each group. Each column with a bar represents the mean ± S.D. *P < 0.01 and **P < 0.05 versus sham groups; #P < 0.05 versus MI + shCtrl group. (For interpretation of the references to colour in this figure legend, the reader is referred to the Web version of this article.)

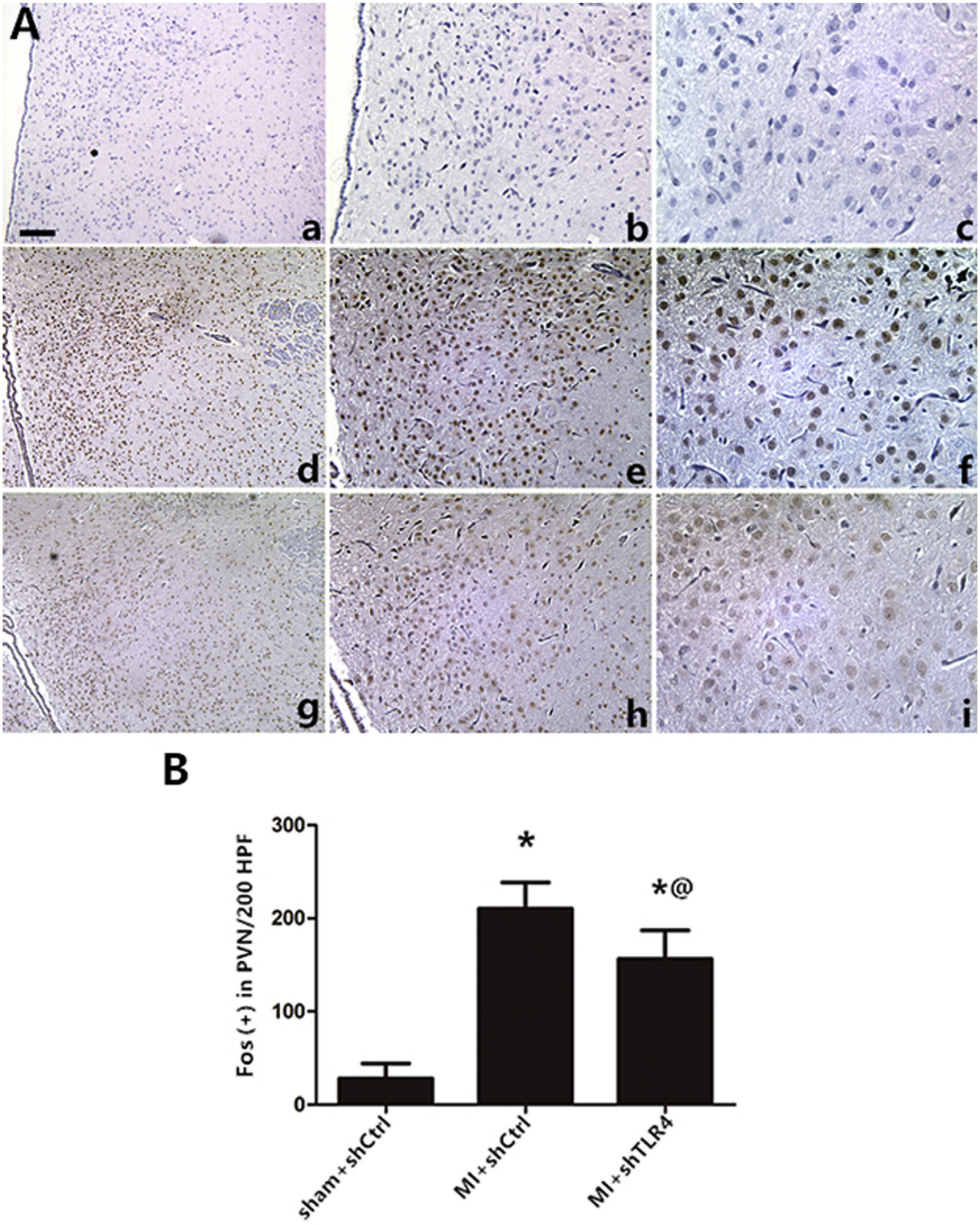

Fig. 5. (A) Representative immunohistochemical images of sympathetic nerve activity at three days post-MI, as indicated by the activation marker of the neurons Fos family (brown), and nuclei (blue) were stained with hematoxylin in a (magnification × 100), b (× 200), c (× 400): the sham + shCtrl group; d (× 100), e (× 200), f (× 400): the MI + shCtrl group; g (× 100), h (× 200), i (× 400): the MI + shTLR4 group. n = 10–11 in each group. The data are expressed as the mean ± S.D. Bar = 50 μm *P < 0.01 versus sham group; @P < 0.05 versus MI + shCtrl group. (For interpretation of the references to colour in this figure legend, the reader is referred to the Web version of this article.)

(Abcam, 1:2000), anti-IL-1β rabbit polyclonal (Abcam, 1:1000), anti-TNF-α rabbit polyclonal (Abcam, 1:1000), anti-Histone 3 rabbit polyclonal (Goodbio Technology, Wuhan, China; 1:1000) and anti-GAPDH mouse polyclonal (Goodbio Technology, 1:1000) antibodies at 4 °C overnight. Membranes were then incubated with HRP-conjugated anti-rabbit or anti-mouse secondary Abs (GenScript, Piscataway, NJ, USA; 1:5000) at 37 °C for 1 h, and detected with the ECL (Millipore, Billerica, MA, USA) method in a FluroChem E Imager (ProteinSimple, Santa

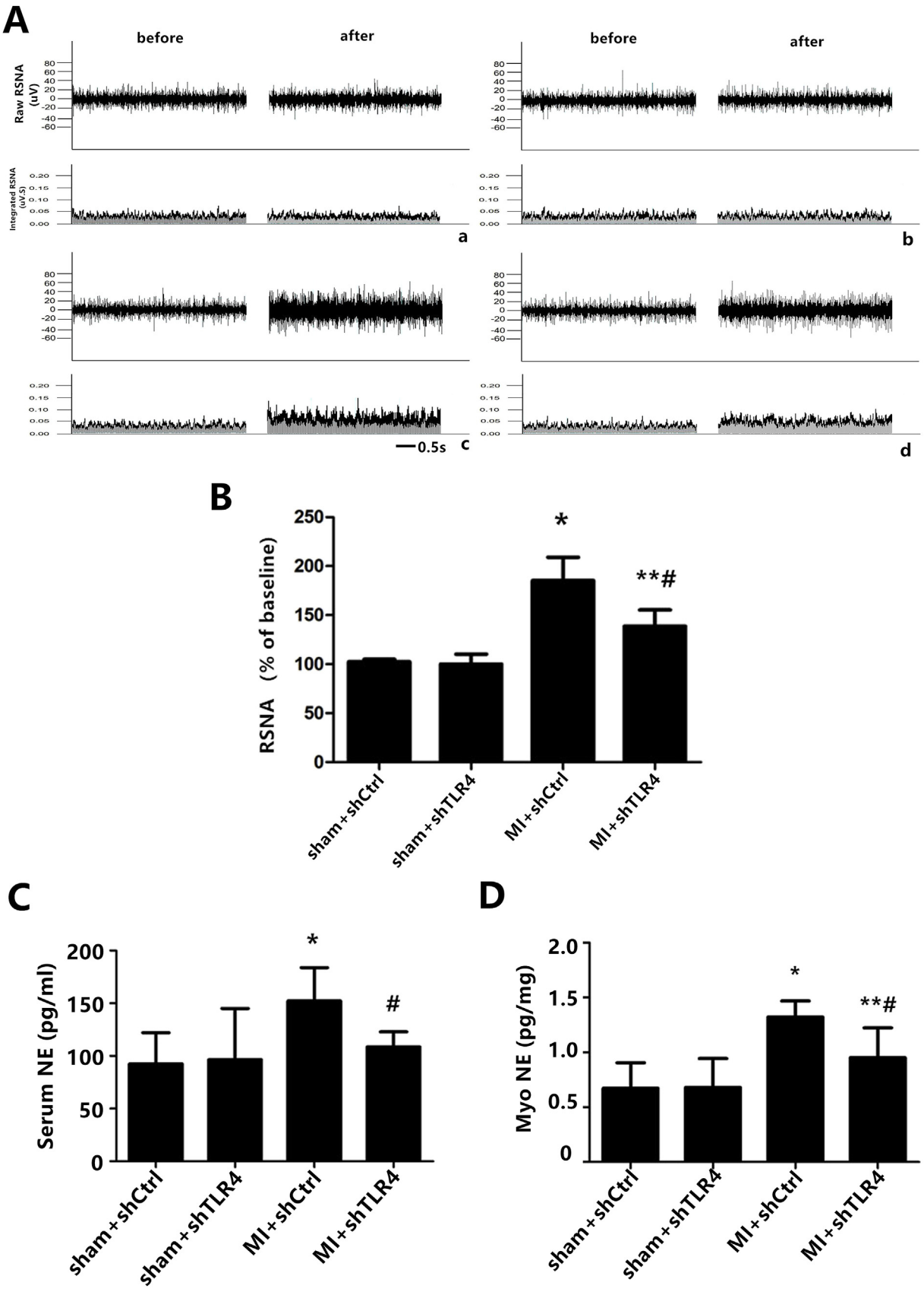

Fig. 6. (A) Direct recordings of raw RSNA and integrated RSNA from the rats in the sham + shCtrl (a), sham + shTLR4 (b), MI + shCtrl (c), MI + shTLR4 (d) groups. The cytokine levels of NE from the serum (C) and myocardium tissue (D) as measured by ELISA. The results are shown as the mean ± S.D. in the two independent experiments. n = 7–9 in each group. *P < 0.01 and **P < 0.05 versus sham groups; #P < 0.05 versus MI + shTLR4 group.

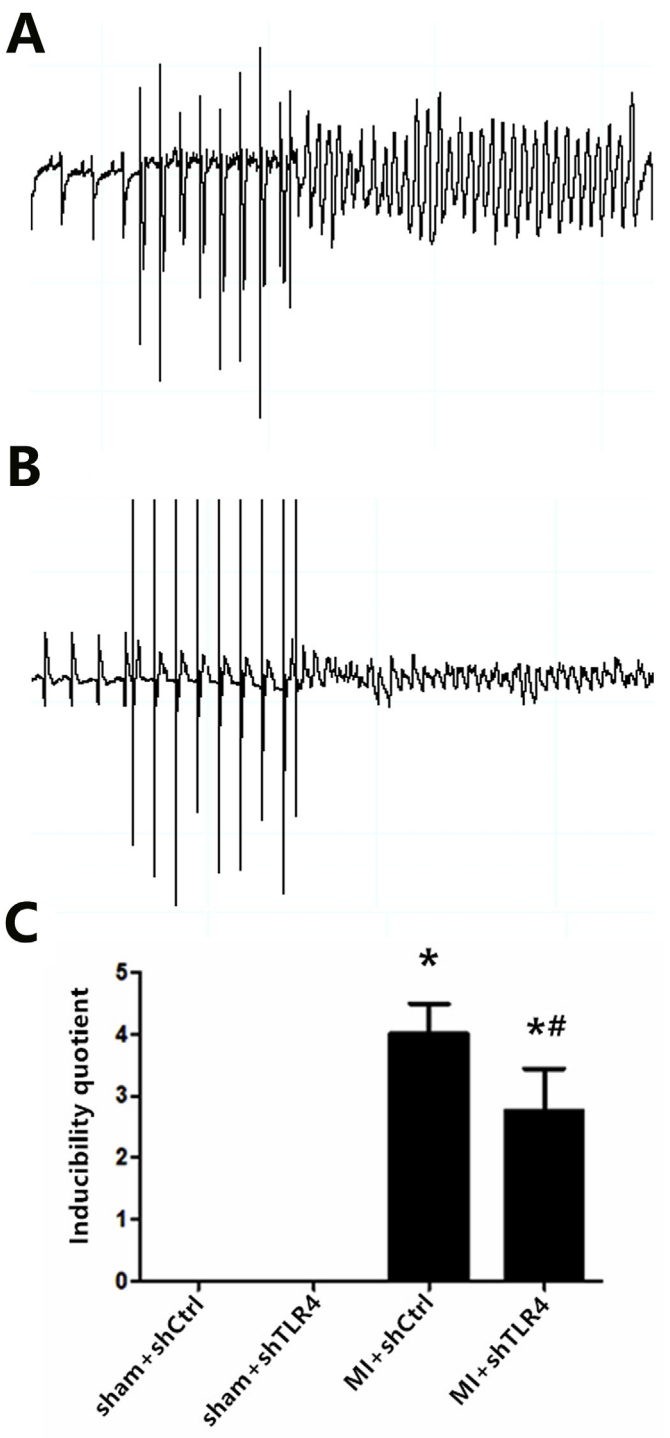

Fig. 7. (A) Programmed electrical stimulation at three days post-MI: Ventricular tachycardia (A) and ventricular fibrillation (B). (C) Recordings of typical inducible VAs. Comparisons of the arrhythmia scores among four groups. n = 7–8 in each group. *P < 0.01 compared with sham groups; #P < 0.05 compared with MI + shCtrl group.

Clara, Calif., USA). NIH Image J software (National Institutes of Health, Bethesda, MD, USA) was used to analyze the densities relative to GAPDH or Histone 3.

2.11. Enzyme-linked immunosorbent assay (ELISA)

A double-antibody sandwich ELISA kit (Cusabio Biotech Co, Wuhan, China) was used to detect the concentration of IL-1β, TNF-α, and the excitatory neurotransmitter, norepinephrine (NE), to represent sympathetic nerve activity. All the procedures were performed according to the manufacturer's instructions. The NE in serum is reported in pg/ml plasma, while NE tissue concentration is reported in pg/mg myocardium tissue. Each treatment was repeated three times. The OD values were detected by microplate reader at a wavelength of 450 nm, and the mean values of these molecules in different groups were compared statistically.

2.12. Statistics

Quantitative data are presented as mean ± SD. More than two groups were compared in the experiments via ANOVA followed by Tukey's test. Analyses were conducted with SPSS 19.0 (SPSS Inc., Chicago, IL, USA). A P-value < 0.05 was considered statistically significant.

3. Results

3.1. TLR4, NF-κB, and ROS production were increased in rats post- MI

The successful establishment of an infarct can be confirmed by ST wave elevation in ECG, regional cyanosis, and observation of a thinner wall area via Masson's trichrome staining (see supplemental figures). The results of Masson's trichrome staining revealed that the infarcted area was larger in the MI surgery groups compared with the sham groups (P < 0.05). However, no marked differences were observed in the MI and MI-intervention rats. The temporal patterns of TLR4, NF-κB, IκB-α, and NOX2 (a membrane-associated oxidase protein) expression in the PVN were detected by Western blotting post-MI. TLR4 protein started to up-regulated as early as 1 day after ligation of the coronary artery although we did not note the significant difference in statistic, and remained at a high level after 7 days (Fig. 1B). Parallel increases in the expression of NF-κB and NOX2 were also detected and reached a peak between 3 and 5 days (Fig. 1D and E). IκB-α synthesis was decreased over a similar time period after AMI (Fig. 1C).

3.2. Local knockdown of TLR4 inhibited NF-κB expression and ROS formation after MI induction

To reveal the role of TLR4 in the pathogenesis of MI, AAV-shRNA was microinjected into the PVN as described in protocol 2. The microscopic detection of GFP expression in the PVN of experimental animals was used to evaluate the distribution of the delivered virus. Our results indicated that the shRNA complex was efficiently delivered *in vivo* via PVN microinjection after 4 weeks (see supplemental figures). Overall, 157 of the 181 rats were included (three were excluded due to infarct area limitation and 21 died). Western blotting revealed that infarction induced higher protein expression of TLR4 in the cytoplasm and increased NF-κB and decreased IκB-α levels in nuclei (Fig. 2B–E). In addition, higher levels of IL-1β and TNF-α were measured by ELISA (Fig. 2F and G), indicating that MI induced NF-κB nuclear translocation in an IκB-α-dependent manner. The administration of TLR4 shRNA efficiently inhibited the degradation of IκB-α and prevented the translocation of NF-κB into the nucleus in the MI rat. Simultaneously, ROS generation were detected via lucigenin chemiluminescence and DHE. MI rats had a significantly higher accumulation of ROS in the PVN as compared to those from sham groups. Following PVN microinjection of shRNA TLR4, this change in MI rats was attenuated (Fig. 3).

3.3. TLR4 was activated predominantly in microglia within the PVN in MI rats

A similar pattern of tendency of TLR4 expression was noted by immunofluorescence. Ionized calcium-binding adapter molecule-1 (Iba-1)-positive staining was measured to quantify the degree of

Table 1
Protocol 2 HRV measurements at the end of study.

Parameters	Sham		Ligation	
	Sham + shCtrl	Sham + shTLR4	MI + shCtrl	MI + shTLR4
No. of surviving rats	36	37	43	41
HR, bpm	395 ± 10.2	409 ± 14	443 ± 18.5*	422 ± 13.2*,#
MAP, mm Hg	115.24 ± 3.0	103.8 ± 4.7	91.7 ± 7.7*	92.1 ± 7.9
LF,nu	22.52 ± 3.18	20.64 ± 4.01	41.24 ± 6.06*	33.91 ± 3.58*,#
HF, nu	88.21 ± 3.52	83.96 ± 4.38	70.00 ± 5.21*	77.89 ± 5.09*
LF/HF	0.2462 ± 0.05	0.2232 ± 0.03	0.5774 ± 0.03*	0.4179 ± 0.04*,#

Values are mean ± SD.
HR, heart rate; MAP, mean arterial pressure; LF, low frequency; HF, high frequency; LF/HF, low frequency/high frequency.
*$p < 0.05$ compared with sham groups.
#$p < 0.05$ compared with group MI + shCtrl.

inflammatory microglia infiltration during infarction. Iba-1 expression was increased significantly after MI and was slightly attenuated in the MI + shRNA TLR4 group (the difference was not statistically significant), indicating that TLR4 silencing may play a role in the activation of microglia during MI. Nearly all of the TLR4 was expressed in microglia in the PVN area at the early inflammatory stage of MI rats, as confirmed via double-staining of Iba-1-positive microglia and TLR4 (Fig. 4).

3.4. TLR4 was involved in sympathetic hyperactivity post-MI

To assess the effect of TLR4 inhibition on sympathetic nerve activity, we quantified interrelated measurements in the central and peripheral nervous systems. Immunohistochemical staining of Fos family members including Fos-B, Fra-1, and Fra-2, as an indicator of neuronal activation, demonstrated that MI induced widespread and significant neuronal activation throughout the PVN with little Fos protein expression in other brain areas at the level of the PVN. In addition, down-regulation of Fos protein expression was observed following administration of TLR4 shRNA (Fig. 5). The trend in Fos family expression was used to assess the role of TLR4 in central neuronal activity, which is a precondition of peripheral sympathetic hyperactivity. Physiologically, neural factors, which promote excitatory activity or decrease inhibitory neurotransmission in the PVN, have been shown to increase sympathoexcitation [29]. The current study showed that MI could induce an increase in NE, suggesting an indirect representation of the augmentation of sympathetic activity, both in the plasma and myocardium. NE levels in the inhibition group were significantly decreased compared with MI only rats (Fig. 6C and D). In the MI and intervention groups, NE levels mirrored those of RSNA content (Fig. 6B), both of which reflect sympathetic nerve activity. Higher ventricular arrhythmia scores, suggesting sympathetic nerve hyperactivity, were also observed via electrical stimulation (Fig. 7). We used 24-h continuous ECG recordings acquired with radiotelemetry to search for the presence and pattern of an autonomic imbalance. The ratio of LF to HF was analyzed, and the HR was notably down-regulated in the MI-shRNA TLR4 rats versus the MI rats (Table 1).

3.5. TLR4 induced sympathetic hyperactivity via an NF-κB dependent pathway and ROS production

In protocol 3, a real control group (naïve group) was utilized to exclude the potential effects of microinjection itself. No significant difference was observed between the naïve group and the sterile saline group. The mechanism of TLR4 role in sympathetic nerve activity was investigated by the administration of LPS, a specific agonist for TLR4. LPS priming alone significantly increased levels of NF-κB, the pro-inflammatory cytokines IL-1β and TNF-α (Fig. 8C, D, and G), and decreased IκB-α expression in naïve rats (Fig. 8B). PDTC, a metal chelator and antioxidant, can inhibit the activation of NF-κB specifically by suppressing the release of the inhibitory subunit IkB from the latent cytoplasmic form of NF-κB. NOX2, a subunit of the NADPH oxidase, was down-regulated following administration of PDTC (Fig. 8E). LPS markedly induced higher RSNA ($P < 0.01$, Fig. 9B) as well as NE levels in the plasma and myocardial tissue (Fig. 9C and D). Administration of PDTC changed the significant trends measured above and resulted in a favorable outcome in relieving sympathetic hyperactivity.

4. Discussion

Several studies have amassed evidence that inflammation induced by microglia located within the PVN, an important contributor to sympathoexcitation in cardiovascular diseases, participates in sympathetic hyperactivity following myocardial infarction [7,8]. However, the detailed mechanism has not been fully established. The present study demonstrated that TLR4 can be activated in microglia post-MI, and inhibition of TLR4 in the PVN ameliorates sympathoexcitation; and this process is partly associated with the NF-κB pathway and oxidative stress.

Rapid life-threatening VAs, including VT and/or VF, are the major cause of death following AMI [30]. In the chronic stage of MI, ventricular arrhythmias occur due to cardiac sympathetic hyperinnervation because nerve growth factor (NGF) induced by inflammation is elevated [31]. Circumstances are different in the early stage of MI, where increased sympathetic nerve activity is associated with decreased myocardial oxygen supply, damaged myocardium, and anxiety. A 100-fold increase in extracellular catecholamines within the ischemic zone 15 min after ischemia has been reported in previous studies. Catecholamine hypersensitivity is responsible for electromechanical instability and ventricular arrhythmia [32].

Recent findings from others showed that pro-inflammatory cytokines (PICs) produced in the PVN contribute to sympathoexcitation in MI rats [33]. However, individual cytokine inhibition is not markedly effective in attenuating sympathetic hyperactivity [34], because several PICs are activated during the pathological process of MI. Therefore, the current study investigated NF-κB, one of the most important contributors to the production of PICs. Our previous study showed that NF-κB is highly activated at sites of cardiac infarction, which leads to activation of the inflammatory response and sympathetic nerve sprouting [35]. Kang et al. [23] observed that RSNA was increased with NF-κB activation within the PVN in a heart failure (HF) model. Another study demonstrated that inhibition of NF-κB with SN50 (a selective inhibitor of NF-κB) in the PVN decreased NE, glutamate (both are indirect indicators of sympathetic activity), and NAD(P)H oxidase-dependent oxidative stress in HF rats [36]. These results are in accordance with the current results showing that inhibition of NF-κB via PDTC decreased ROS production and RSNA.

TLRs are considered a major component of the innate immune

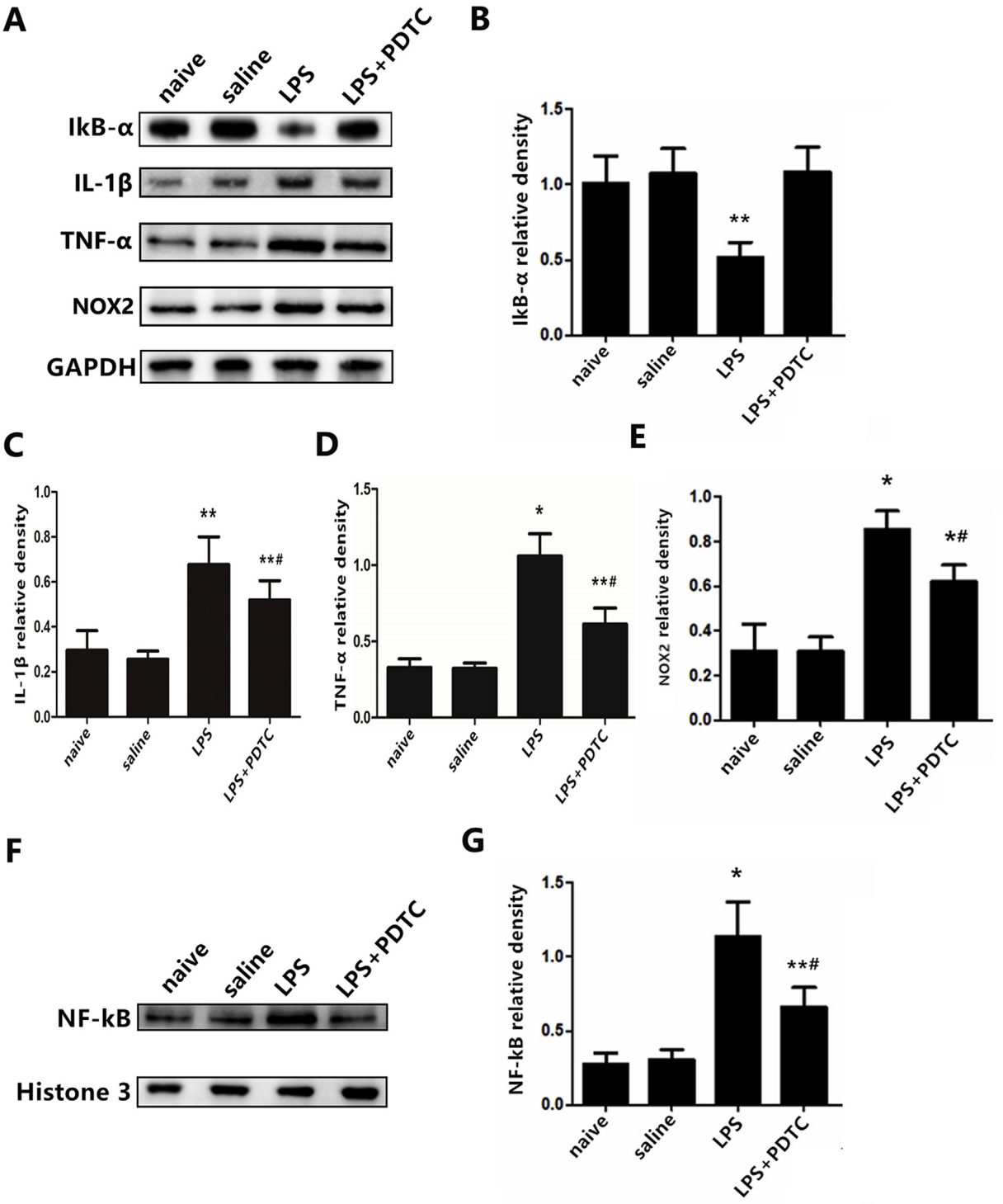

Fig. 8. (A) Representative protein expression levels of NF-κB (65 kD), IκB-α(36 kD), IL-1β (17 kD), TNF-α(16 kD), and NOX2 (60 kD) as determined by western blot. n = 11–12 in each group.*P < 0.01 and **P < 0.05 versus naïve group; #P < 0.05 versus LPS group.

system, belonging to the pathogen recognition receptors family [11,12]. There are 13 TLRs found in mammals, and each has a distinct function in innate immune recognition [37]. According to TLRs subcellular localization, we classified them into two groups: TLR1, TLR2, TLR4-6, and TLR11 are expressed on the plasma membrane, whereas others are located in the endosome [38]. TLR4 is one of the most important upstream molecules of NF-κB and is found in many types of cells like macrophages, hepatocytes, and renal tubular cells [39–41]. In the central nervous system (CNS), TLR4 is expressed primarily in microglia and sparsely in astrocytes and neurons [42]. Double immunostaining of TLR4 and Iba-1, a surface marker of microglia, showed that TLR4 expression increased markedly in microglial cells, indicating its involvement post-MI. Simultaneously, knockdown of TLR4 slightly decreased the degree of microglial activation, which is similar to previous studies showing that direct TLR4 activation promotes PVN microglial activation [10]. This suggests that TLR4 is a contributor to the activation of microglia. A previous study reported that ICV microinjection of LPS, a specific ligand for TLR4 [43], elicits sympathetic hyperactivity via PICs

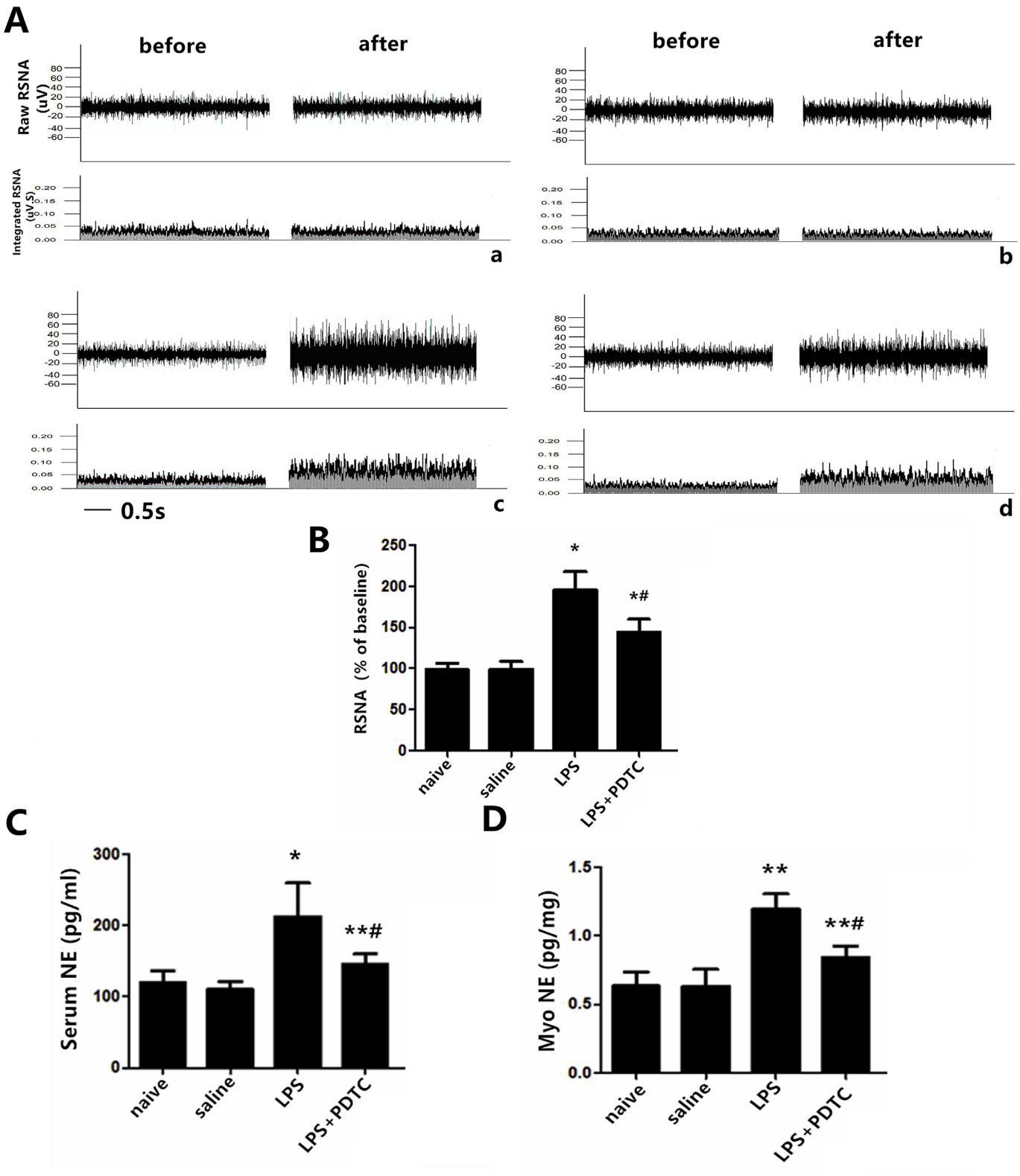

Fig. 9. (A) Direct recordings of raw RSNA and integrated RSNA from rats in the naïve group (a), saline group (b), LPS group (c), LPS + PDTC group (d). The cytokine levels of NE from serum (C) and myocardium tissue (D) as measured by ELISA. The data are expressed as the mean ± S.D. of two experiments. n = 11–12 in each group. *P < 0.01 and **P < 0.05 compared with the naïve group; #P < 0.05 compared with the LPS group.

production [44]. Another study demonstrated that PVN treatment with VIPER (viral inhibitory peptide of TLR4) caused a dramatic reduction in plasma levels of NE in hypertensive rats [45]. To determine the effects of activated TLR4 on sympathetic nerve activity post-MI, TLR4 shRNA was administered in the present study. shRNA technology is superior because the protective effects in experimental animals are ensured, and stable results may be acquired for longer-term inhibition in *vivo*. Following MI, an increase in RSNA (which is representative of enhanced

peripheral sympathetic activity) and increased HRV (which may indicate dysfunction of the cardiac autonomic nervous system) was observed. Because MI-induced VAs are related to cardiac sympathetic overdrive, the NE content in the myocardium was analyzed. Knockdown of TLR4 induced a reduction of NE in the myocardium, and the ventricular arrhythmia score was reduced, supporting the concept that the VF threshold can be reduced when confronted with a sympathetic blockade or vagal up-regulation in animal studies [46]. All of the above studies suggested that upregulation of brain TLR4 plays a critical role in sympathetic hyperactivity.

Zimmerman et al. [47] demonstrated that ROS, a vital signal factor within the PVN, plays an important role in cardiovascular diseases like HF and hypertension through activation of the sympathetic nervous system. One previous study reported that dose-dependent renal sympathoinhibitory, hypotensive, and bradycardic responses were observed after ICV administration of a ROS scavenger [21]. In addition, a previous study found that ROS production induced by AngII administration were almost entirely absent in TLR4-deficient compared with TLR4-sufficient mice [48], suggesting that TLR4 plays a critical role in mediating ROS production. NAD(P)H oxidase family enzymes are one of the main sources of ROS. Among NOX enzymes, NOX2 (also named gp91phox) plays an important role in ROS overproduction [49]. The current study showed that inhibition of TLR4 or NF-κB attenuated the NF-κB-dependent inflammatory response and the expression of NOX2 in the PVN. We can deduce that TLR4/NF-κB contributes to a sustained increase in oxidative stress in the PVN, and blockade of this within the PVN might open new beneficial insights in therapeutic approaches to prevent fetal complications post-MI.

Numerous studies from others demonstrated this relevant pathway in other cardiovascular diseases: increased activation of TLR4 can lead to the induction of oxidative stress. Furthermore, oxidation of phospholipids causes TLR4 to sense ROS production and increase the former's expression [50]. NF-κB is the most important contributor in the activation of PICs and ROS secretion. The latter increases the activity of NF-κB in turn [5,51,52], and the interplay between TLR4/NF-κB and ROS may result in activation of neurons in the CNS and increased NE secretion, thereby contributing to the aggravation of ventricular arrhythmias in the pathological process of MI. Individual inhibition of these components alleviates, but cannot normalize, the pressure of injury from VAs post-MI. However, the current study did not take further investigation about the crosstalk among these molecules in our present study.

TLR4 can be stimulated by endogenous signals of tissue injury, including debris from apoptotic and necrotic cells, oligosaccharides, heat shock proteins, and nucleic acid fragments [13,14]. High mobility group box-1 (HMGB1) is one of the most important endogenous ligands that participates in various inflammatory conditions. When injury or infection occurs, HMGB1 is actively released by immune cells like microglia into the extracellular space and reacts to an inflammatory response [53–55]. Our recent study has demonstrated that HMGB1 was increased in PVN and participated in sympathetic hyperactivity post-MI [56], which led to the hypothesis that HMGB1 may be one of the contributors in the activation of the TLR4/NF-κB signaling pathway and ROS production post-MI. However the source of ROS production requires further investigation. Another study reported that vascular adhesion molecules such as selectins and integrins can be secreted by ischemic heart tissue, which contributes to an increase in the permeability of the blood-brain barrier (BBB) [57]. Therefore, it is possible that other known ligands of TLR4, like debris from apoptotic and necrotic cells, come into contact with TLR4 in the brain tissue through the bloodstream in the early stages of MI.

Outlook

The present study focused specifically on the role of TLR4 expressed on microglia within the PVN during sympathoexcitation in AMI rats. Although sympathetic hyperactivity induced by NF-κB or oxidative stress has already been determined in HF models [23,25], the present study is the first investigation showing that activated microglia within the PVN can participate in sympathetic hyperactivity via the TLR4/NF-κB signaling pathway post-MI. Our data provide a possible strategy by which secondary damage could be partly relieved after MI. Future studies are warranted that focus on the specific mechanism of microglial TLR4 activation and other neuroactive substances like ROS within the PVN in the early stages of MI. Simultaneously, PVN microglial targeted TLR4 knockout rats were applied.

Limitations

First, there are potential limitations inherent in extrapolating data from rats to humans. Second, myocardial infarction induces activation of microglia in the PVN, periaqueductal gray (PAG), rostral ventrolateral medulla (RVLM), and nucleus tractus solitarius (NTS), and area postrema (AP) [58], indicating that there are multiple cardio-relevant nuclei participating in sympathetic activation. Therefore, knocking down TLR4 in the PVN cannot exclude the function of other cardiovascular nuclei in the CNS. Third, TLR4 is not only expressed in microglia but neurons and astrocytes; we did not determine whether other cell types have any role on sympothoexcitation. Fourth, shRNA-specific TLR4-knockdown relieves sympathetic hyperactivity post-MI; however, we did not investigate whether the use of the shRNA technique may affect other normal functions of TLR4 in the inflammatory response. Nonetheless, the results of our study suggest a significant role for the TLR4 pathway in life-threatening arrhythmias following MI.

5. Conclusions

Overall, the present study demonstrated that TLR4 activation augmented sympathetic nerve activity following myocardial infarction via microglial NF-κB activation and ROS production in the PVN. Inhibition of TLR4 attenuated sympathoexcitation, providing new insights into the mechanisms in CNS activation of the sympathetic nerve system. Based on current findings, TLR4 might be a potential target for the modulation of NF-kB and oxidative stress in sympathetic hyperactivity post-MI.

Conflicts of interest

None.

Acknowledgements

This work was supported by the National Natural Science Foundation of China (NSFC, No. 81870253 and 81600265), Clinical Medical Science and Technology Innovation Plan of Jinan (No. 201602173).

Appendix A. Supplementary data

Supplementary data to this article can be found online at https://doi.org/10.1016/j.redox.2019.101186.

References

[1] M. Kalla, N. Herring, Cardiac sympatho-vagal balance and ventricular arrhythmia, Auton. Neurosci. 199 (2016) 29–37.
[2] P.J. Podrid, T. Fuchs, R. Candinas, Role of the sympathetic nervous system in the genesis of ventricular arrhythmia, Circulation 82 (Suppl 2) (1990) I103–I113.
[3] J.F. Thayer, S.S. Yamamoto, J.F. Brosschot, The relationship of autonomic imbalance, heart rate variability and cardiovascular disease risk factors, Int. J. Cardiol. 141 (2010) 122–131.
[4] C. Capone, G. Faraco, J.R. Peterson, C. Coleman, J. Anrather, T.A. Milner, V.M. Pickel, R.L. Davisson, C. Iadecola, Central cardiovascular circuits contribute to the neurovascular dysfunction in angiotensin II hypertension, J. Neurosci. Off. J. Soc. Neurosci. 32 (2012) 4878–4886.

[5] Y.M. Kang, Y. Ma, J.P. Zheng, C. Elks, S. Sriramula, Z.M. Yang, J. Francis, Brain nuclear factor-kappa B activation contributes to neurohumoral excitation in angiotensin II-induced hypertension, Cardiovasc. Res. 82 (2009) 503–512.

[6] Kc, T.E. Dick, Modulation of cardiorespiratory function mediated by the paraventricular nucleus, Respir. Physiol. Neurobiol. 74 (1·2) (2010) 55–64 1.

[7] Z. Shi, X.B. Gan, Z.D. Fan, et al., Inflammatory cytokines in paraventricular nucleus modulate sympathetic activity and cardiac sympathetic afferent reflex in rats, Acta Physiol. 203 (2011) 289–297.

[8] Y. Yu, Z.H. Zhang, S.G. Wei, et al., Brain perivascular macrophages and the sympathetic response to inflammation in rats after myocardial infarction, Hypertension 55 (2010) 652–659.

[9] F.L. Rock, G. Hardiman, J.C. Timans, R.A. Kastelein, J.F. Bazan, A family of human receptors structurally related to drosophila toll, Proc. Natl. Acad. Sci. U. S. A. 95 (1998) 588–593.

[10] G.S. Masson, A.R. Nair, R.B. Dange, P.P. Silva-Soares, L.C. Michelini, J. Francis, Toll-like receptor 4 promotes autonomic dysfunction, inflammation and microglia activation in the hypothalamic paraventricular nucleus: role of endoplasmic reticulum stress, PLoS One 10 (2015) e0122850.

[11] H.J. Anders, D. Schlöndorff, Toll-like receptors: emerging concepts in kidney disease, Curr. Opin. Nephrol. Hypertens. 16 (2007) 177–183.

[12] H.J. Anders, Toll-like receptors and danger signaling in kidney injury, J. Am. Soc. Nephrol. 21 (2010) 1270–1274.

[13] D. Verzola, A. Bonanni, A. Sofia, F. Montecucco, E. D'Amato, V. Cademartori, E.L. Parodi, F. Viazzi, C. Venturelli, G. Brunori, Toll-like receptor 4 signalling mediates inflammation in skeletal muscle of patients with chronic kidney disease, J. Cachexia Sarcopenia Muscle 8 (1) (2017) 131–144.

[14] J.R. Caso, J.M. Pradillo, O. Hurtado, et al., Toll-like receptor 4 is involved in brain damage and inflammation after experimental stroke, Circulation 115 (2007) 1599–1608.

[15] S. Alfonso-Loeches, M. Pascual-Lucas, A.M. Blanco, et al., Pivotal role of TLR4 receptors in alcohol-induced neuroinflammation and brain damage, J. Neurosci. 30 (2010) 8285–8295.

[16] R. Gorina, M. Font-Nieves, L. Marquez-Kisinousky, et al., Astrocyte TLR4 activation induces a proinflammatory environment through the interplay between MyD88-dependent NF-kB signaling, MAPK, and Jak1/Stat1 pathways, Glia 59 (2011) 242–255.

[17] M.C. Zimmerman, E. Lazartigues, J.A. Lang, P. Sinnayah, I.M. Ahmad, D.R. Spitz, R.L. Davisson, Superoxide mediates the actions of angiotensin II in the central nervous system, Circ. Res. 91 (2002) 1038–1045.

[18] F. Megumi, A. Katsuyuki, N. Ai, F. Toshiro, Sympathoexcitation by oxidative stress in the brain mediates arterial pressure elevation in salt-sensitive hypertension, Hypertension 50 (2007) 360–367.

[19] T. Shokoji, A. Nishiyama, Y. Fujisawa, H. Hitomi, H. Kiyomoto, N. Takahashi, S. Kimura, M. Kohno, Y. Abe, Renal sympathetic nerve responses to Tempol in spontaneously hypertensive rats, Hypertension 41 (2003) 266–273.

[20] H. Xu, G.D. Fink, J.J. Galligan, Nitric oxide-independent effects of Tempol on sympathetic nerve activity and blood pressure in DOCA-salt rats, Am. J. Physiol. Heart Circ. Physiol. 283 (2002) H885–H892.

[21] N. Lu, B.G. Helwig, R.J. Fels, S. Parimi, M.J. Kenney, Central Tempol alters basal sympathetic nerve discharge and attenuates sympathetic excitation to central ANG II, Am. J. Physiol. Heart Circ. Physiol. 287 (6) (2004) H2626–H2633.

[22] K. Asehnoune, D. Strassheim, S. Mitra, J.Y. Kim, E. Abraham, Involvement of reactive oxygen species in Toll-like receptor 4-dependent activation of NF-kappa B, J. Immunol. 172 (2004) 2522–2529.

[23] Y.M. Kang, Y. Ma, C. Elks, J.P. Zheng, Z.M. Yang, J. Francis, Cross-talk between cytokines and reninangiotensin in hypothalamic paraventricular nucleus in heart failure: role of nuclear factor-kappaB, Cardiovasc. Res. 79 (2008) 671–678.

[24] J. Sun, X.S. Ren, Y. Kang, et al., Intermedin in Paraventricular Nucleus Attenuates Sympathoexcitation and Decreases TLR4-Mediated Sympathetic Activation via Adrenomedullin Receptors in Rats with Obesity-Related Hypertension, Neurosci Bull 35 (2019) 34–46, https://doi.org/10.1007/s12264-018-0292-9.

[25] J. Qi, X.J. Yu, X.L. Shi, et al., NF-κB blockade in hypothalamic paraventricular nucleus inhibits high-salt-induced hypertension through NLRP3 and caspase-1, Cardiovasc. Toxicol. 16 (2016) 345–354.

[26] G. Paxinos, C. Watson, The Rat Brain in Stereotaxic Coordinates, Elsevier Academic Press, New York, 2005.

[27] T. Radovits, S. Korkmaz, S. Loganathan, et al., Comparative investigation of the left ventricular pressure-volume relationship in rat models of type 1 and type 2 diabetes mellitus, Am. J. Physiol. Heart Circ. Physiol. 297 (2009) 8.

[28] R.M. Lataro, L.E.V. Silva, C.A.A. Silva, et al., Baroreflex control of renal sympathetic nerve activity in early heart failure assessed by the sequence method, J. Physiol. 595 (11) (2017 Jun 1) 3319–3330, https://doi.org/10.1113/JP274065.

[29] K.P. Patel, B. Xu, X. Liu, N.M. Sharma, H. Zheng, Renal denervation improves exaggerated sympathoexcitation in rats with heart failure: a role for neuronal nitric oxide synthase in the paraventricular nucleus, Hypertension 68 (2016) 175–184.

[30] H.J. Arevalo, F. Vadakkumpadan, E. Guallar, et al., Arrhythmia risk stratification of patients after myocardial infarction using personalized heart models, Nat. Commun. 7 (2016) 11437.

[31] J. Yin, Y. Wang, H. Hu, et al., P2X7 receptor inhibition attenuated sympathetic nerve sprouting after myocardial infarction via the NLRP3/IL-1β pathway, J. Cell Mol. Med. 21 (2017) 2695–2710.

[32] A.A. Hasanien, B.J. Drew, Prevalence and prognostic significance of long QT interval in patients with acute coronary syndrome: review of the literature, J. Cardiovasc. Nurs. 29 (2014) 271–279.

[33] D. Du, M. Jiang, M. Liu, et al., Microglial P2X$_7$ receptor in the hypothalamic paraventricular nuclei contributes to sympathoexcitatory responses in acute myocardial infarction rat, Neurosci. Lett. 587 (2015) 22–28.

[34] D.L. Mann, J.J. McMurray, M. Packer, K. Swedberg, J.S. Borer, W.S. Colucci, et al., Targeted anticytokine therapy in patients with chronic heart failure: results of the Randomized Etanercept Worldwide Evaluation (RENEWAL), Circulation 109 (2004) 1594–1602.

[35] Y. Wang, F. Suo, J. Liu, et al., Myocardial infarction induces sympathetic hyperinnervation via a nuclear factor-kappaB-dependent pathway in rabbit hearts, Neurosci. Lett. 535 (2013) 128–133.

[36] Yu-Ming Kang, Feng Gao, Hui-Hua Li, Jeffrey P. Cardinale, Carrie Elks, Wei-Jin Zang, Xiao-Jing Yu, Yan-Yan Xu, Jie Qi, Qing Yang, Joseph Francis, NF-κB in the paraventricular nucleus modulates neurotransmitters and contributes to sympathoexcitation in heart failure, Basic Res. Cardiol. 106 (6) (2011 Nov) 1087–1097.

[37] R. Medzhitov, Toll-like receptors and innate immunity, Nat. Rev. Immunol. 1 (2001) 135–145.

[38] S. Akira, Toll receptor families: structure and function, Semin. Immunol. 16 (2004) 1–2.

[39] H. Wu, G. Chen, K.R. Wyburn, J. Yin, P. Bertolino, J.M. Eris, S.I. Alexander, A.F. Sharland, S.J. Chadban, TLR4 activation mediates kidney ischemia/reperfusion injury, J. Clin. Invest. 117 (2007) 2847–2859.

[40] M. Yamamoto, S. Sato, H. Hemmi, S. Uematsu, K. Hoshino, T. Kaisho, O. Takeuchi, K. Takeda, S. Akira, TRAM is specifically involved in the Toll-like receptor 4-mediated MyD88- independent signaling pathway, Nat. Immunol. 4 (2003) 1144–1150.

[41] Y. Zhai, X.D. Shen, R. O'Connell, F. Gao, C. Lassman, R.W. Busuttil, G. Cheng, J.W. KupiecWeglinski, Cutting edge: TLR4 activation mediates liver ischemia/reperfusion inflammatory response via IFN regulatory factor 3-dependent MyD88-independent pathway, J. Immunol. 173 (2004) 7115–7119.

[42] H. Lee, S. Lee, I.H. Cho, S.J. Lee, Toll-like receptors: sensor molecules for detecting damage to the nervous system, Curr. Protein Pept. Sci. 14 (2013) 33–42.

[43] Y.C. Lu, W.C. Yeh, P.S. Ohashi, LPS/TLR4 signal transduction pathway, Cytokine 42 (2008) 145–151.

[44] Z.H. Zhang, Y. Yu, S.G. Wei, et al., Centrally administered lipopolysaccharide elicits sympathetic excitation via NAD(P)H oxidase-dependent mitogen activated protein kinase signaling, J. Hypertens. 28 (2010) 806–816.

[45] R.B. Dange, D. Agarwal, R. Teruyama, J. Francis, Toll-like receptor 4 inhibition within the paraventricular nucleus attenuates blood pressure and inflammatory response in a genetic model of hypertension, J. Neuroinflammation 12 (2015 Feb 18) 31.

[46] F. Lombardi, R.L. Verrier, B. Lown, Relationship between sympathetic neural activity, coronary dynamics, and vulnerability to ventricular fibrillation during myocardial ischemia and reperfusion, Am. Heart J. 105 (1983) 958–965.

[47] M.C. Zimmerman, E. Lazartigues, R.V. Sharma, R.L. Davisson, Hypertension caused by angiotensin II infusion involves increased superoxide production in the central nervous system, Circ. Res. 95 (2004) 210–216.

[48] K. Ogawa, Y. Hirooka, T. Kishi, T. Ide, K. Sunagawa, Partially silencing brain toll like receptor 4 prevents in part left ventricular remodeling with sympathoinhibition in rats with myocardial infarction-induced heart failure, PLoS One 8 (2013) e69053.

[49] S.R. Datla, K.K. Griendling, Reactive oxygen species, NADPH oxidases, and hypertension, Hypertension 56 (2010) 325–330.

[50] P.S. Tawadros, K.A. Powers, M. Ailenberg, S.E. Birch, J.C. Marshall, K. Szaszi, et al., Oxidative stress increases surface toll-like receptor 4 expression in murine macrophages via ceramide generation, Shock 44 (2015) 157–165.

[51] J.P. Cardinale, S. Sriramula, N. Mariappan, D. Agarwal, J. Francis, Angiotensin II-induced hypertension is modulated by nuclear factor-kB in the paraventricular nucleus, Hypertension 59 (2012) 113–121.

[52] Y. Hirooka, Role of reactive oxygen species in brainstem in neural mechanisms of hypertension, Auton. Neurosci. 142 (2008) 20–24.

[53] M.E. Bianchi, DAMPs, PAMPs and alarmins: all we need to know about danger, J. Leukoc. Biol. 81 (2007) 1–5.

[54] M.T. Lotze, K.J. Tracey, High-mobility group box 1 protein (HMGB1): nuclear weapon in the immune arsenal, Nat. Rev. Immunol. 5 (2005) 331–342.

[55] A.M. Piccinini, K.S. Midwood, DAMPening inflammation by modulating TLR signalling, Mediat. Inflamm. 2010 (2010) 6723951-21.

[56] P Li, Y Jie, S YuGen, et al., High mobility group box-1 in hypothalamic paraventricular nuclei attenuates sympathetic tone in rats at post-myocardial infarction, Cardiol J. (2018 Oct 19), https://doi.org/10.5603/CJ.a2018.0117 [Epub ahead of print].

[57] Y.H. Hsieh, K. McCartney, T.A. Moore, et al., Intestinal ischemia-reperfusion injury leads to inflammatory changes in the brain, Shock 36 (4) (2011 Oct) 424–430.

[58] M. Dworak, M. Stebbing, A.R. Kompa, et al., Sustained activation of microglia in the hypothalamic PVN following myocardial infarction, Auton. Neurosci. 169 (2012) 70–76.